Chapter 4

Constraining Neutrino mass using the large scale H I distribution in the post-reionization epoch *

4.1 Introduction

It has been established from neutrino oscillation experiments that neutrinos have mass. There are profound implications of these particles being massive and cosmological observations are expected to put strong constrains on neutrino physics. Several cosmological probes are used in this regard [11]. We believe that at least two of the three species of neutrinos are non-relativistic today.

The standard Big bang cosmological model predicts a neutrino background. In the early Universe, neutrinos are in thermal equilibrium with the primordial plasma through weak interactions. The neutrino decoupling happens at z_{dec} when the weak interaction rate equals the Hubble expansion. A direct detection of the neutrino background is very difficult. However, the presence of Neutrinos affect the clustering of matter through gravitational instability in an expanding Universe Neutrinos are expected to be in thermal equilibrium with CMBR in the early Universe whereby they contribute as radiation to the energy density of the Universe and their number is fixed. Accordingly their fractional contribution to the present day matter budget is given by $f_\nu = \frac{\Omega_\nu}{\Omega_m}$ where $\Omega_\nu = \sum_i m_i/93.14h^2\text{eV}$ [181, 182] with m_i denoting the mass of each neutrino species. When the temperature of

*Based on the paper Constraining neutrino mass using the large-scale HI distribution in the post-reionization epoch, **Ashis Kumar Pal**, Tapomoy Guha Sarkar, Monthly Notices of the Royal Astronomical Society, Volume 459, Issue 4, 11 July 2016, Pages 3505-3511

the universe is very high they can be treated as a part of radiation and after the CMB temperature drops below their masses, they can contribute to the matter density of the Universe. The free streaming of neutrinos causes them to wipe out fluctuations on scales smaller than the scale corresponding to the horizon size at the epoch when the neutrinos became non-relativistic.

After thermal decoupling of the neutrinos, they constitute a collisionless fluid, where the individual particles free-stream with a characteristic thermal velocity v_{th}. We can think of v_{th} as denoting an average free-streaming speed. Similar to the definition of the Jeans length scale we can define the neutrino free-streaming scale as [183]

$$k_{fs}(z) = \left(\frac{4\pi G\bar{\rho}a^2(t)}{v_{th}^2(t)}\right)^{1/2} \tag{4.1}$$

The free-streaming comoving vector may be simplified as

$$k_{fs} = \sqrt{\frac{3}{2}}H(z)/v_{th}(1+z) \tag{4.2}$$

When neutrinos are relativistic, this coincides with the horizon scale, and when neutrinos become non-relativistic at $z = z_{nr}$ [12] $v_{th} \sim \langle p\rangle/m_\nu$ and the free streaming scale becomes

$$k_{nr} \sim \sqrt{\frac{3}{2}}\frac{H(z_{nr})m_\nu}{3T_\nu(z_{nr})(1+z_{nr})}.$$

For modes $k < k_{nr}$ neutrinos behave like usual dark matter and there is no suppression of power. Modes with $k > k_{fs}$ have neutrino perturbations wiped out and consequently CDM power spectrum is also suppressed.

Cosmological measurement of neutrino mass [149, 170, 184–191] depends directly on the level of precision at which this suppression of power in the matter power spectrum can be detected. Whereas CMBR gives stringent constraints on neutrino mass [192–196] it is necessary to obtain measurements from the low redshift Universe. Matter power spectrum for $z < 1$ is highly non-linear and neutrino mass measurements have degeneracies with competition from dark energy [197]. While Galaxy surveys are traditionally used to put bounds on neutrino masses, we propose the cross-correlation of the 21-cm signal with the Lyman-α forest as a competitive probe of neutrino cosmology.

Mapping the neutral hydrogen distribution (HI) in the post-reionization epoch using the observation of the redshifted 21 cm signal towards measurement of the matter power spectrum has been studied as a means to measure neutrino mass

[186, 193, 198–201]. At redshifts $z < 6$, HI responsible for the 21 cm signal lies predominantly in the Damped Lyman Alpha (DLA) clouds [80] and the diffuse collective 21 cm emission from these clouds form a background in radio observations. The redshifted 21-cm diffuse emission from the post-reionization epoch is well modelled using a constant neutral fraction [83, 84], and a bias function [23, 24]. The diffuse neutral gas distribution in the same redshift range can also be probed using the distinct absorption features of the Lyman-α forest [136]. Large astrophysical foregrounds [13–18] come in the way of detecting the 21 cm signal. The cross correlation of the 21 cm signal with other cosmological probes like the Lyman-α forest and Lyman-Break galaxies, has been proposed as a viable way [19–21] to mitigate the effect of foregrounds. The flux through the Lyman-α forest and the redshifted 21 cm signal can both be modelled as biased tracers of the underlying dark matter distribution and are expected to be correlated [22–25]. The cross-correlation signal is a direct probe of the matter power spectrum over a large redshift range in the post reionization epoch.

In this chapter we investigate the constraints on total neutrino mass using the cross correlation of the Lyman-α forest and the 21-cm signal from the post reionization epoch. The suppression of power on scales $k > k_{nr}$ allows us to constrain the neutrino mass. In this chapter we constrain the parameters Ω_m and Ω_ν using the cross-correlation signal. These are the only two free parameters in our analysis. The values of $\Omega_\Lambda = 0.685, \Omega_b h^2 = 0.02222, h = 0.6731, n_s = 0.9655, \sigma_8 = 0.829$ are fixed to their fiducial values as obtained from ([196]Table 4: TT + lowP) for this analysis. Ω_K varies but is not treated as a free independent parameter. We consider a future radio interferometric observation of the 21 cm using a telescope like SKA1-mid [*] and a BOSS [†] like Lyman-α forest survey for obtaining predictions for bounds on the parameters.

4.2 Cross correlation signal and estimation of Neutrino mass

The cross-correlation of the redshifted 21-cm signal and the transmitted flux through the Lyman-α forest has been proposed and studied as a cosmological probe of structure formation and background evolution in the post-reionization epoch [20]. We saw in the last chapter that though the two signals owe their ori-

[*] https://www.skatelescope.org/
[†] https://www.sdss3.org/surveys/boss.php

gins to H I in distinct astrophysical systems at redshifts $z \leq 6$ but are expected to be correlated on large scales.

Bulk of the HI in the post-reionization epoch is believed to be housed in the dense self-shielded DLA systems. These clumps are the dominant source of the 21-cm emission in this epoch. The signal from individual DLA sources is rather weak and resolving individual sources is also rather unfeasible. The collective emission from the clouds, however form a diffuse background in all radio observations at observing frequencies less than 1420 MHz. Tomographic imaging using the low resolution intensity mapping of this diffuse background radiation is a potentially rich probe of cosmology [75, 79, 102, 104, 107, 110, 112, 124].

Along a line of sight $\hat{\mathbf{n}}$ traversing a HI cloud at redshift z the CMBR brightness temperature changes from T_γ to $T(\tau_{21})$ owing to the emission/absorption corresponding to the spin flip Hyperfine transition at $\nu_e = 1420$ MHz in the rest frame of the gas. The quantity of interest in radio observations at a frequency $\nu = \nu_e/(1+z)$ is the excess brightness temperature $T_b(\hat{\mathbf{n}}, z)$ redshifted to the observer at present. This is given by

$$T_b(\hat{\mathbf{n}}, z) = \frac{T(\tau_{21}) - T_\gamma}{1+z} \approx \frac{(T_s - T_\gamma)\tau_{21}}{1+z}. \tag{4.3}$$

Writing $\mathbf{r} \equiv (r\hat{\mathbf{n}}, z)$, where r is the comoving distance corresponding to z, we have the fluctuations in $T_b(\hat{\mathbf{n}}, z)$ given by $\delta_T(\mathbf{r}) = \bar{T}(z) \times \eta_{\rm HI}(\mathbf{r})$ [27] , where

$$\bar{T}(z) = 4.0{\rm mK}(1+z)^2 \left(\frac{\Omega_{b0}h^2}{0.02}\right)\left(\frac{0.7}{h}\right)\left(\frac{H_0}{H(z)}\right) \tag{4.4}$$

and

$$\eta_{HI}(r\hat{\mathbf{n}}, z) = \bar{x}_{HI}(z)\left\{\left(1 - \frac{T_\gamma}{T_s}\right)\left[\delta_H(z, \hat{\mathbf{n}}) - \frac{1+z}{H(z)}\frac{\partial v}{\partial r}\right] + \frac{T_\gamma}{T_s} s\delta_H(\hat{\mathbf{n}}r, z)\right\} \tag{4.5}$$

Here $\bar{x}_{HI}(z)$ denote the mean neutral fraction, $\delta_H(z, \hat{\mathbf{n}})$ denotes the HI density fluctuations and s is a function that takes into account the fluctuations of the spin temperature assuming it to be related to the HI fluctuations. The peculiar velocity of the gas, v introduces the anisotropic term $(1+z)/H(z)\frac{\partial v}{\partial r}$.

In the post reionization epoch one has $T_\gamma/T_s << 1$ whereby the 21 cm signal is seen in emission and we have

$$\eta_{HI}(r\hat{\mathbf{n}}, z) = \bar{x}_{HI}(z)\left[\delta_H(z, \hat{\mathbf{n}}) - \frac{1+z}{H(z)}\frac{\partial v}{\partial r}\right]. \tag{4.6}$$

In Fourier space the fluctuation in 21-cm excess brightness temperature $\delta_T(\mathbf{r})$ is

denoted by $\Delta_T(\mathbf{k})$ and is given by

$$\Delta_T(\mathbf{k}) = C_T[1 + \beta_T \mu^2]\Delta(\mathbf{k}) \tag{4.7}$$

where $\Delta(\mathbf{k})$ is the Fourier transform of the dark matter over density δ and we have assumed that the peculiar velocity is sourced by dark matter over density. The quantity β_T is the redshift space distortion [202] parameter and $\mu = \hat{\mathbf{n}} \cdot \hat{\mathbf{k}}$. The redshift dependent quantity C_T is given by $C_T = \bar{T}(z)\bar{x}_{HI}(z)b_T$ where b_T denotes a bias that relates the HI fluctuations in Fourier space $\Delta_H(\mathbf{k})$ to the underlying dark matter fluctuations $\Delta(\mathbf{k})$ as $\Delta_H(\mathbf{k}) = b_T\Delta(\mathbf{k})$. The 21 cm bias has been studied in several independent studies [24, 93, 96]. We have discussed the nature of H I bias in the second chapter. We adopt a linear bias model [24] in this work. It is important to note that in cosmologies with massive neutrinos HI is more clustered. This is an additional effect which occurs because we fundamentally believe that the gas is contained in halos and halos are rarer in models with neutrino mass and are thereby more biased [203]. This enhances the 21-cm power spectrum by a roughly scale independent factor of 1.15 at $z = 2.5$ [204].

Whereas the dense clumpy HI sources the 21 cm emission, the diffuse intergalactic HI in the post reionization epoch also produces distinct absorption lines in the spectra of background quasars namely the Lyman-α forest [151, 166]. The 21 cm signal and the Lyman-α forest arises from two distinct astrophysical systems. The Lyman-α forest, consists of absorption lines in the Quasar spectra which originates from tiny fluctuations in the low density diffuse HI along the line of sight. The Flux $\mathcal{F}$ through the Lyman-α forest is modeled using the fluctuating Gunn-Peterson approximation [49, 171]

$$\frac{\mathcal{F}}{\bar{\mathcal{F}}} = \exp^{-A(1+\delta)^\alpha} \tag{4.8}$$

where α is related to the slope of the temperature density relationship γ as $\alpha = 2 - 0.7(\gamma - 1)$, and A [166] is a redshift dependent parameter depending on several astrophysical and cosmological parameters like the photo-ionization rate, IGM temperature and the evolution history [137, 147]. The relationship between the observed flux through the Lyman-α forest and the underlying dark matter distribution is non-linear[205]. However, on large scales the smoothed Lyman-α forest flux traces the dark matter fluctuations [172–174] via a bias. The precise analytic understanding about the bias is not very robust and has been studied under certain approximations. However, a linear bias model is largely supported

by numerical simulations of the Lyman-α forest [22].

The fluctuations of the flux through the Lyman-α forest $\Delta_{\mathcal{F}}$ can hence be related to the dark matter fluctuations in Fourier space as

$$\Delta_{\mathcal{F}}(\mathbf{k}) = C_{\mathcal{F}}[1 + \beta_{\mathcal{F}}\mu^2]\Delta(\mathbf{k}) \tag{4.9}$$

The parameters $(C_{\mathcal{F}}, \beta_{\mathcal{F}})$ are independent of one another and depend on A, γ and the flux probability distribution function. The predictions for $\beta_{\mathcal{F}}$ from particle-mesh simulations indicate that increasing the smoothing length has the effect of lowering the value of $\beta_{\mathcal{F}}$ which is ideally set by choosing the smoothing scale at the Jean's length which is in turn sensitive to the IGM temperature. We adopt the values $(C_{\mathcal{F}}, \beta_{\mathcal{F}}) = (-0.15, 1.11)$ from simulations of Lyman-α forest [22]. It is important to note that $\beta_{\mathcal{F}}$ can not be interpreted like β_T for the 21-cm signal where it was related to the bias b_T.

Being tracers of the underlying dark matter distribution the Lyman-α forest and 21 cm signal are correlated on large scales. The cross correlation of the Lyman-α forest and the 21cm signal has been proposed as a cosmological probe [19, 20]. Apart from mitigating the serious issue of 21 cm foregrounds, the cross correlation if detected, ascertains the cosmological origin of the signal as opposed to the auto correlation 21 cm signal. Several advantages of the cross-correlation have been studied in earlier works [20] (discussed in the last chapter). The 3D cross correlation power spectrum is given by

$$\langle \Delta_{\mathcal{F}}(\mathbf{k})\Delta_T^*(\mathbf{k}')\rangle = (2\pi)^3\delta^3(\mathbf{k} - \mathbf{k}')P_{\mathcal{F}T}(\mathbf{k}), \tag{4.10}$$

with

$$P_{\mathcal{F}T}(\mathbf{k}) = C_{\mathcal{F}}C_T(1 + \beta_{\mathcal{F}}\mu^2)(1 + \beta_T\mu^2)P(\mathbf{k}). \tag{4.11}$$

where $P(\mathbf{k})$ is the dark matter power spectrum.

Observationally the Lyman-α forest survey as well as radio observations of the 21 cm signal will probe certain volumes of the Universe. The cross-correlation can however be computed only in the overlapping region denoted by $\mathcal{V}$. The Lyman-α surveys typically shall cover a larger volume and thus $\mathcal{V}$ is set by the 21-cm observations. If B be the observational bandwidth of the 21 cm observation and if $\theta_a \times \theta_a$ is the angular patch that the radio telescope probes, then

$$\mathcal{V} = B\frac{dr}{d\nu} \times r^2\theta_a^2. \tag{4.12}$$

The observed 21 cm signal denoted by Δ_{TO} shall include a noise term and may be written as

$$\Delta_{T0}(\mathbf{k}) = \Delta_T(\mathbf{k}) + \Delta_{NT}(\mathbf{k}) \tag{4.13}$$

Similarly the observed Lyman-α forest transmitted flux fluctuation in Fourier space may be written as

$$\Delta_{\mathcal{F}o}(\mathbf{k}) = \int \tilde{\rho}(\mathbf{k}-\mathbf{K})\Delta_{\mathcal{F}}(\mathbf{K})\ d^3\mathbf{K} + \Delta_{N\mathcal{F}}(\mathbf{k}) \tag{4.14}$$

which involves a convolution of the three dimensional field with a normalized sampling function in Fourier space $\tilde{\rho}(\mathbf{k})$, and $\Delta_{N\mathcal{F}}(\mathbf{k})$ denotes a pixel noise contribution. The sampling function relates the one dimensional Lyman-α forest skewers to the 3D field and is given by

$$\rho(\mathbf{r}) = \frac{1}{N}\sum_i w_i \delta_D^2(\mathbf{r}_\perp - \mathbf{r}_{\perp i}) \tag{4.15}$$

with a set of weight functions w_i that are used to maximize the SNR and N is used to normalize $\int \rho(\mathbf{r}) d^3\mathbf{r} = 1$. The sum extends over all the QSO locations $\mathbf{r}_{\perp i}$ in the field. The error in measurement of the cross power spectrum is hence given by $\delta P_{\mathcal{F}T}(\mathbf{k})^2 = \sigma^2_{\mathcal{F}T}/N_m$, where

$$\sigma^2_{\mathcal{F}T} = \frac{1}{2}\left[P^2_{\mathcal{F}T}(\mathbf{k}) + \left(P_{\mathcal{F}\mathcal{F}}(\mathbf{k}) + P^{1D}_{\mathcal{F}\mathcal{F}}(k_\parallel)P^{2D}_w + N_{\mathcal{F}}\right)\ (P_{TT}(\mathbf{k}) + N_T)\right] \tag{4.16}$$

where $P^{1D}_{\mathcal{F}\mathcal{F}}(k_\parallel)$ denotes the one dimensional power spectrum of Lyman-α forest flux fluctuations

$$P^{1D}_{\mathcal{F}\mathcal{F}}(k_\parallel) = \frac{1}{(2\pi)^2}\int d^2\mathbf{k}_\perp P_{\mathcal{F}\mathcal{F}}(\mathbf{k}). \tag{4.17}$$

Here N_T and $N_{\mathcal{F}}$ denotes the noise power spectrum for 21 cm observation and the Lyman-α forest respectively and P^{2D}_w denotes the power spectrum of the weight functions. The quantity N_m is the number of available Fourier modes and is given by

$$N_m(k,\mu) = \frac{2\pi k^2 \mathcal{V} dk d\mu}{(2\pi)^3}. \tag{4.18}$$

The noise power spectrum for the 21 cm observations and the Lyman-α forest depend on the specific observational parameters. For radio-interferometric observation of the 21 cm signal the noise power spectrum is a function of the mode k being probed and the observation frequency $\nu = 1420\ \mathrm{MHz}/(1+z)$ and is given

by [64, 111]

$$N_T(k,\nu) = \frac{T_{sys}^2}{t_0}\left(\frac{c^2}{\nu^2 A_e}\right)^2 \frac{2r^2}{N_{ant}(N_{ant}-1)f_{2D}(U,\nu)}\frac{dr}{d\nu}. \tag{4.19}$$

where, A_e denotes the effective collecting area of a single antenna, $\mathbf{U} = \mathbf{k}_\perp r/2\pi$ and t_o is the total observation time for a single pointing. The system temperature is denoted by T_{sys}. If N_{ant} denotes the total number of antennae and $f_{2D}(U,\nu)$ [21, 68, 206] is the normalized baseline distribution function.

For the Lyman-α forest observations along multiple sight lines, the noise power spectrum is given by [176] as

$$N_{\mathcal{F}} = \sigma_{\mathcal{F}N}^2/\bar{n} \tag{4.20}$$

where $\bar{n}$ is the average quasar number density in the field given by $\bar{n} = N_Q/r^2\theta_a^2$ for a total of N_Q QSO spectra in the field of view and $\sigma_{\mathcal{F}N}^2$ is the variance of the pixel noise with

$$\sigma_{\mathcal{F}N}^2 = \frac{1}{N_Q}\sum \bar{\mathcal{F}}^{-2}[S/N]_{\Delta x}^{-2}\left(\frac{\Delta x}{1\text{Mpc}}\right). \tag{4.21}$$

where the sum is extended over all the N_Q quasars in the field of view. The signal to ratio S/N in a pixel of size Δx, with Δx matched to the frequency smoothing scale of the 21 cm observation is considered to be held at a constant average value of 3. This is clearly going to lead to an underestimate of the sensitivity, since many quasars shall typically have $SNR > 3$.

To make error estimates for the two parameters Ω_ν and Ω_m we use the Likelihood analysis. For a Gaussian distribution the Likelihood $\mathcal{L}(\lambda|D)$ where $\lambda = (\Omega_\nu, \Omega_m)$ denotes the model vector and D is the data, we may write the Fisher matrix F as

$$F_{rs} = \left\langle \frac{\partial^2 \ln\mathcal{L}}{\partial\lambda_r \partial\lambda_s} \right\rangle \tag{4.22}$$

For a diagonal covariance matrix (variance) the 2×2 Fisher matrix has the elements

$$F_{rs} = \sum_{\mathbf{k}} N_m(\mathbf{k})\frac{1}{\sigma_{\mathcal{F}T}^2}\left(\frac{\partial P_{\mathcal{F}T}}{\partial\lambda_r}\right)\left(\frac{\partial P_{\mathcal{F}T}}{\partial\lambda_s}\right) \tag{4.23}$$

Writing $\mathbf{k} = (k,\mu)$ we may replace the sum by an integral as

$$F_{rs} = \int\int \frac{1}{\sigma_{\mathcal{F}T}^2}\left(\frac{\partial P_{\mathcal{F}T}}{\partial\lambda_r}\right)\left(\frac{\partial P_{\mathcal{F}T}}{\partial\lambda_s}\right)\frac{2\pi k^2 \mathcal{V} dk d\mu}{(2\pi)^3} \tag{4.24}$$

where λ_r and λ_s can take values Ω_ν and Ω_m. The estimator we use is an unbi-

ased estimator and thus we can use the Cramer-Rao bound gives a limit on the theoretical errors on the i^{th} parameter as $\delta\lambda_i = \sqrt{F_{ii}^{-1}}$ which we use in this chapter.

4.3 Results and Discussion

4.3.1 Observational aspects

We have assumed a fiducial cosmological model [196] with

$$(\Omega_\Lambda, \Omega_m, h, n_s) = (0.685,\ 0.315,\ 0.6731,\ 0.9655)$$

for this analysis. The fiducial redshift $z = 2.5$ is chosen since the quasar distribution peaks in the redshift range $2 < z < 3$. At this fiducial redshift the Lyman-α forest spectrum can be measured in an approximate range $\Delta z = 0.43$. This is owing to the fact that part of the quasar spectrum $\sim 10,000$ Km s^{-1} blue-ward of the Lyman-α emission and ~ 1000 Km s^{-1} red-ward of the Lyman-β line has to eliminated to avoid the quasar proximity effect and contamination from Lyman-β and other metal lines respectively. A high quasar density is required for the cross-correlation to be measured at high level of sensitivity. We consider a BOSS like Lyman-α forest survey with a quasar density of 30 deg^{-2} with an average 3σ sensitivity for the measured spectra. The BOSS survey covers a large part of the sky with a transverse coverage of $10,000$deg^2. The volume probed by the Lyman-α forest is hence given by $\frac{c}{H}\Delta z \times r^2\theta^2$ with $\Delta z = 0.43$ and $\theta^2 = 3.043$ rad^2. We note, however that the cross-correlation can only be computed only in the overlapping volume between the Lyman-α forest survey and 21 cm survey volume which is expected to be much smaller.

4.3.2 Telescope parameters

We consider an 21 cm intensity mapping experiment using a radio interferometer with specifications roughly following that of SKA1-mid *. The radio interferometer shall operate in frequency range from 350 MHz to 14 GHz. The fiducial redshift of $z = 2.5$ corresponds to a frequency of ~ 406MHz falls in this frequency range. We assume the array to be composed of a total of 250 dish like antennae. Each individual antenna is of diameter $\sim$ 15m with an antenna efficiency of 0.8. We

*http://www.skatelescope.org/wp-content/uploads/2012/07/SKA-TEL-SKO-DD-001-1_BaselineDesign1.pdf

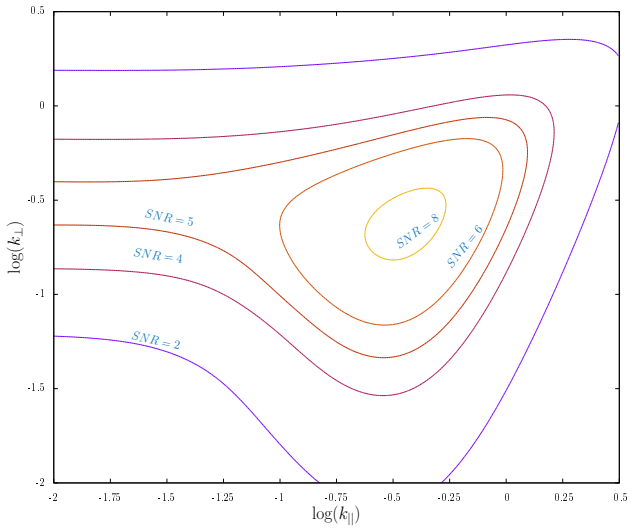

Figure 4.1: Signal to noise ratio for the cross-correlation power spectrum for a single pointing radio observation of 400 hrs. We have considered a QSO density 30 deg^{-2}.

assume that the distribution of the antennae is mostly condensed to a central core with 40%, 55%, 70%, and 100% of the total antennae are within 0.35 km, 1 km, 2.5 km, and 100 km radius respectively with density of antennae falling off radially as an inverse square power law [25]. This allows us to compute the normalized baseline distribution function. It is evident that there can not be any baselines below 30m. Typical intensity mapping experiments aim towards higher power spectrum sensitivity at large scales. The telescope design supports this, since the telescopes are mostly distributed in a central region. The baseline coverage at very small non-linear scales is poor. We assume the system temperature T_{sys} to be 30K at observational frequency of 405.7MHz. Further, the telescope is assumed to have a 32MHz band width.

4.3.3 Results

Figure (4.1) shows the signal to noise ratio for the cross-correlation signal in the $(k_\perp, k_\parallel)$ plane. We have considered a 400 hrs observation of the 21-cm signal in a single pointing of the telescope. We find that a statistically significant detection of the cross-correlation signal at a SNR > 8 is possible in the range $0.19\text{Mpc}^{-1} < k_\parallel <$

0.6Mpc^{-1} and $0.18\text{Mpc}^{-1} < k_{\perp} < 0.36\text{Mpc}^{-1}$. The anisotropy in the $k-$space owes its origin to the redshift space distortion effects and the preferential sensitivity of the noise in the $k-$space. We have assumed here that a perfect foreground subtraction has been achieved. Foreground residuals are expected to degrade the SNR. The issue of foreground removal has been discussed later. The low sensitivity at small baselines owes it origin to cosmic variance whereas the sensitivity at large scales is dictated by instrument noise.

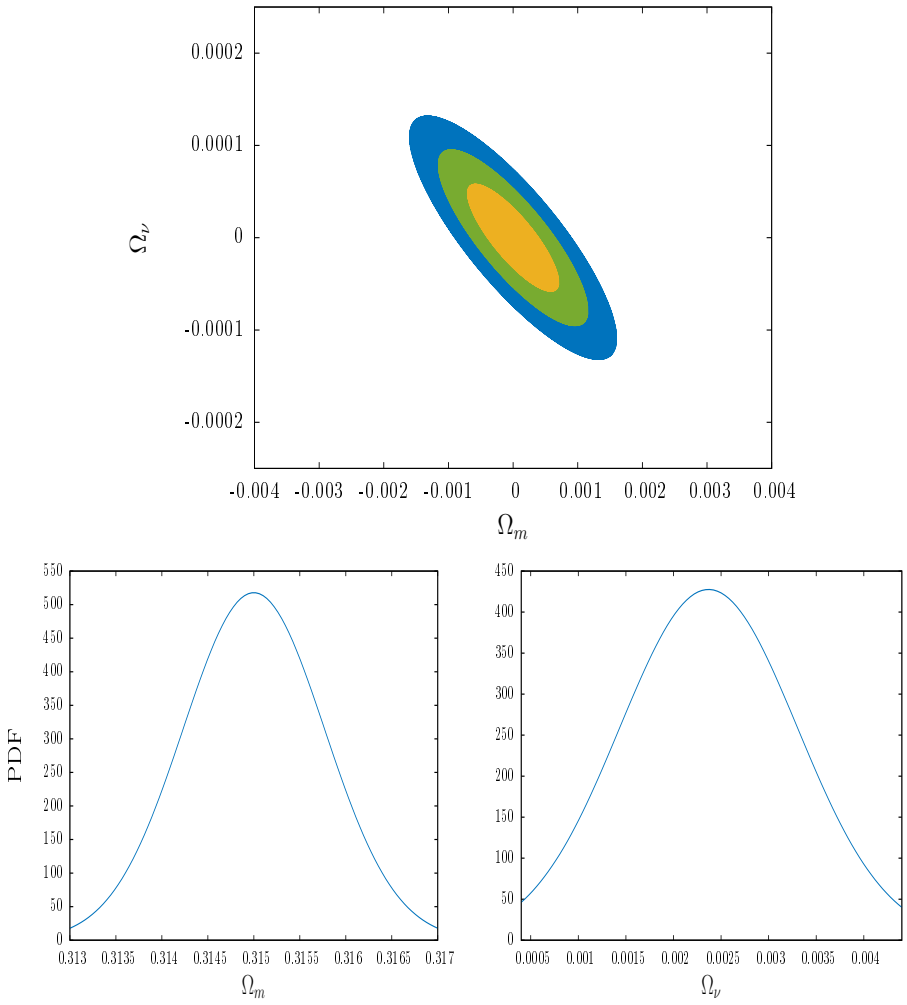

Figure 4.2: 68.3%,95.4% and 99.8% ellipse for 10000 hrs. observations for 25 pointings with each pointing of 400 hrs. The marginalized one dimensional probability distribution function (PDF) for Ω_m and Ω_ν are also shown.

We next, look at the results of the Fisher matrix analysis towards constraining the parameters (Ω_m, Ω_ν). Figure (4.2) shows the confidence ellipses at 68.3%, 95.4% and 99.8% levels. We have considered a total $10,000$ hrs 21 cm observation

Parameter	Fiducial value	% Error 25 pointings	% Error 50 pointings	% Error 100 pointings
Ω_m	0.315	0.361	0.280	0.222
Ω_m	0.315	0.310	0.237	0.184
Ω_m	0.315	0.298	0.227	0.176
Ω_m	0.315	0.296	0.227	0.174
Ω_m	0.315	0.292	0.222	0.171

Table 4.1: 1 σ error for various number of pointings of the 21-cm observation for Ω_m with a total 10,000 hrs observation (distributed equally over the different pointing) of the 21 cm signal

for 25 pointings of radio telescope each corresponding to a 400 hrs observation. The Lyman-α forest survey is assumed to have QSO number density of 30deg^{-2} where each spectrum is measured at an average $> 3-\sigma$ pixel noise level. We find that for these observational parameters, Ω_m and Ω_ν can be measured at 0.29% and 3.25% respectively. Figure (4.2) also shows the marginalized probability distribution for the parameters Ω_m and Ω_ν.

The SKA1-mid kind of radio interferometer considered here has a angular coverage of $2.8 \times 2.8\text{deg}^2$ at redshift of 2.5. This is much smaller than volume covered by the Lyman-α survey. The BOSS Lyman-α survey covers a much larger volume than a typical 21 cm observation. A significant part of the Lyman-α survey volume can be used in the cross-correlation by considering multiple pointings of the radio interferometer. We keep the total observation time fixed at $10,000$ hrs but now consider 50 radio pointings each of 200 hrs duration. Further we consider the possibility of dividing the total observing time into 100 pointings.The results show a clear improvement in the constraints. We tabulate all the results in tables (4.1) and (4.2). This implies that for a QSO survey with a number density $\bar{n} > 30\text{deg}^{-2}$ and with SKA like instrument, it is more advantageous to distribute the total observation time over as many fields of views as possible instead of deep imaging of a single radio field.

Up-to this point our analysis is focused on the estimates of the parameters HI 21 cm intensity mapping using (with SKA1-mid) and Lyman-α (BOSS) surveys, with some specific observational parameters (i.e, QSO density, number of antennae,and time of observations). In the next analysis our interest is focused on the variation of the error estimates if the above mentioned observational parameters are changed

Parameter	Fiducial value	% Error 25 pointings	% Error 50 pointings	% Error 100 pointings
Ω_ν	7.10×10^{-4}	20.70	16.53	13.81
Ω_ν	1.42×10^{-3}	6.47	5.21	4.25
Ω_ν	2.13×10^{-3}	3.73	3.00	2.45
Ω_ν	2.37×10^{-3}	3.25	2.61	2.13
Ω_ν	2.84×10^{-3}	2.57	2.07	1.68

Table 4.2: 1-σ error for various number of pointings for Ω_ν with a total 10,000 hrs observation (distributed equally over the different pointing) of the 21 cm signal.

within the known possible range. We first consider the effect of the variation of number of antennae from 100 to 1000 keeping the time of observation ($t_0 = 400$hrs) and QSO density ($\bar{n} = 30\text{deg}^{-2}$) unchanged. The total 10000 hrs time is hence divided over 25 radio pointings. The collecting area and resolution of the radio telescopes will increase with the number of antennae (keeping the dishes identical). Figure (4.3) shows the $1-\sigma$ error bound on Ω_m, Ω_ν varying with the number of antennas in the radio array. We find that there is no significant improvement in the constraints when number of antennas are increased beyond 350 and, the error bound saturates to a limit set by cosmic variance and the parameters of the Lyman-α survey. The noise contribution from the Lyman-α forest power spectrum measurement depends on the number density of Quasars in the survey. Figure (4.4) represents the improvement of 1σ error in the estimation of parameters due to the of variation QSO density ($\bar{n}$). In this case we find that beyond $\bar{n} > 50$ the decline of the error is very slow and the cosmic variance limit is asymptotically reached.

4.3.4 Optimal strategy

For a more practical scenario it is useful to investigate the optimal observational strategy. We characterize the radio observation with the time of observation and Lyman-α forest survey with the quasar number density in the survey with high SNR spectra. Figures (4.5) and (4.6) shows the contours of constant 1 σ errors of Ω_m, Ω_ν for a single pointing radio observation. The bottom left in each figure corresponds to large observational noise owing to small quasar number density and small time of observation. The top right corner corresponds to large quasar density and long duration radio observation. The error in the parameters show a decrease

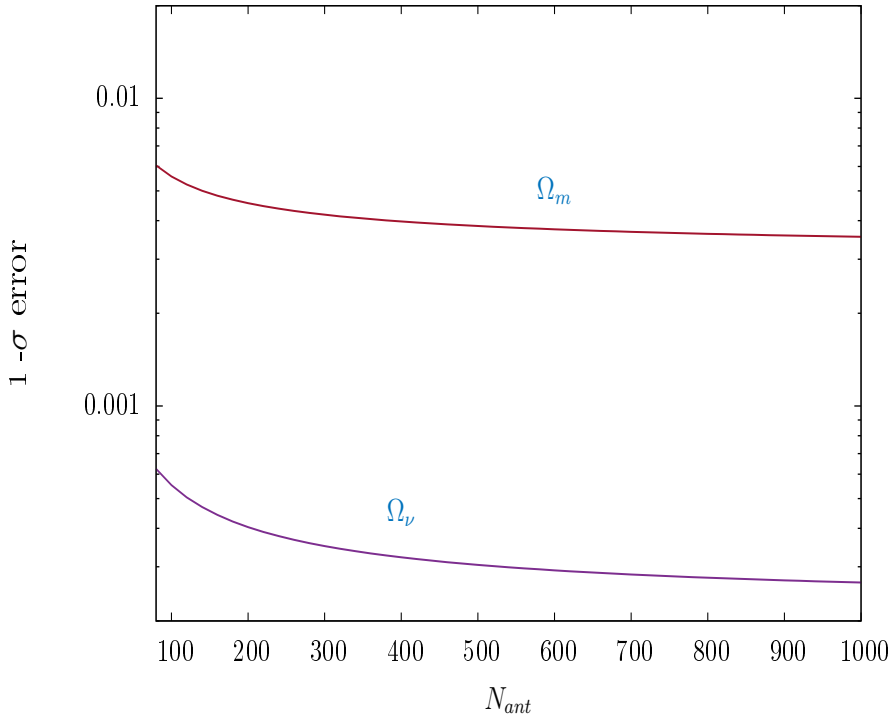

Figure 4.3: Variation of $1-\sigma$ error of the parameters Ω_m and Ω_ν with N_{ant} the number of antennas in the radio-interferometric array.

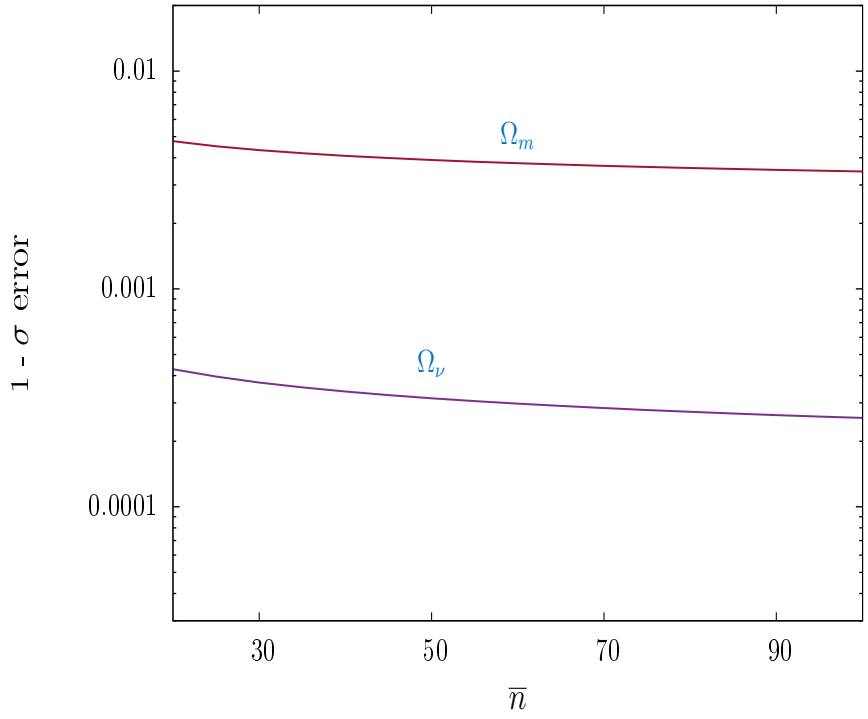

Figure 4.4: Variation of $1-\sigma$ error of the parameters Ω_m and Ω_ν with $\bar{n}$ (deg^{-2}) .

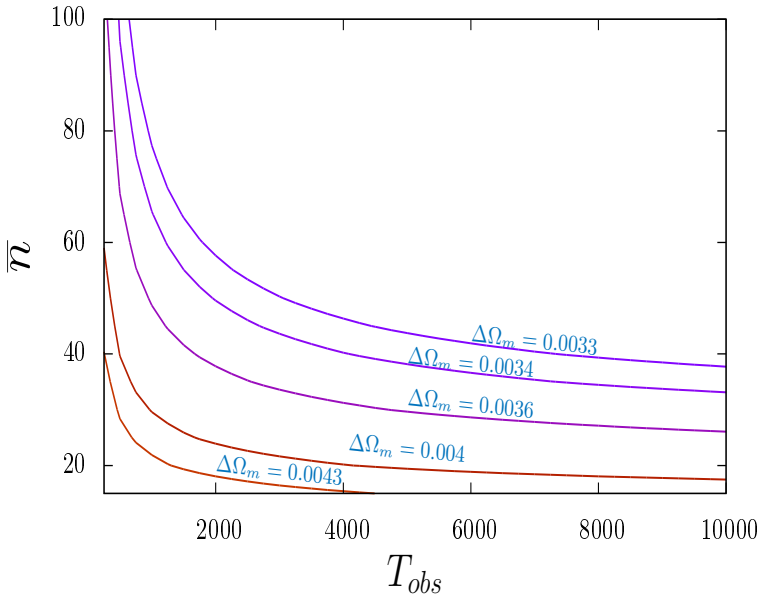

Figure 4.5: Ω_m contours in the $\bar{n}$ and time of observation plane.

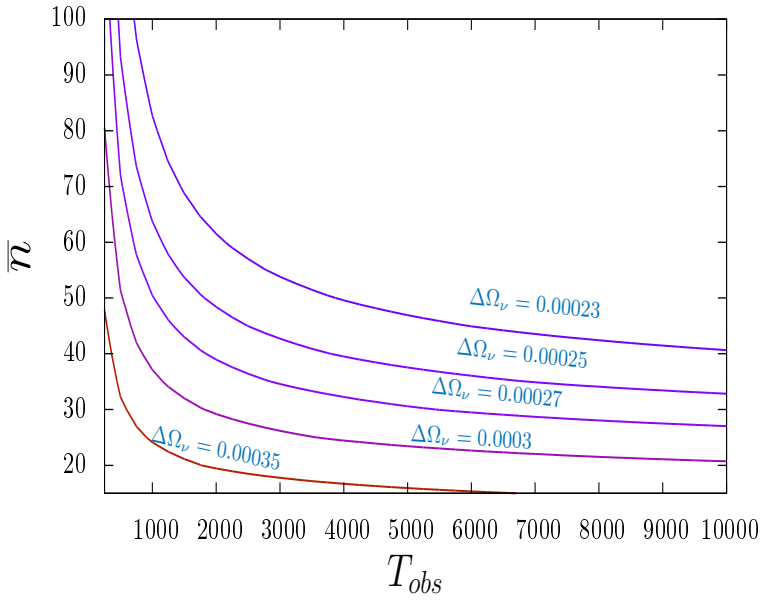

Figure 4.6: Ω_ν contours in the $\bar{n}$ and time of observation plane.

as one moves from the bottom left to the top right corner through the contours. However, beyond a point there is no further improvement and this corresponds to the cosmic variance limit. In this limit the parameter Ω_m can be measured at a 0.9% level and Ω_ν can be measured at 7.6%. Further improvement is only possible through increase of the number of pointings which increases the survey volume and the errors scale as $\sim 1/\sqrt{N_{poin}}$. A total of 25,000 hrs radio observation distributed equally over 25 pointings and a Lyman-α survey with $\bar{n} = 60\text{deg}^{-2}$ will allow Ω_ν to be measured at a 2.26% level. This corresponds to a measurement of $\sum m_\nu$ at the precision of (100 ± 2.26)meV and f_ν at 2.49%. Our general observation is that there should be greater emphasis of increasing survey volumes through bigger bandwidths or using smaller dishes and considering multiple fields of views against extremely deep surveys in small fields. This shall make the constraints parameters stronger. We however note that 25,000 hrs observation in 25 pointings is a rather unfeasible observational strategy. In this idealized survey it is possible to even look into the mass hierarchy for neutrinos. However, Several observational issues poses severe problems towards detection of the signal. The crucial issue as regarding the 21 cm signal, is the issue of foregrounds. Foregrounds like the

galactic synchrotron radiation and extra galactic point sources are several orders of magnitude larger than the cosmological 21 cm signal. Further, man made RFIs [116] also contaminate the signal severely. Several foreground subtraction methods have been proposed. We note that though foreground subtraction is crucial towards measuring the 21 cm signal, these contaminants appear as noise in the cross-correlation and foreground residuals even of the same order of magnitude as the signal shall not entirely inhibit the detection of the cross-correlation signal unlike the unlike the auto correlation. Assuming a fiducial model with $\sum m_\nu = 0.1\text{eV}$ we find that if we have a foreground residual of the 21-cm signal at 200% of the signal itself then the constraint on Ω_ν degrades from 2.26% to 2.7%. Further, if the Lyman-α forest pixel noise is at $1-\sigma$, the constraint on neutrino mass degrades to $\sim 6\%$.

The Lyman-α forest surveys require very high SNR measurement of a large number of spectra for high precision detection of the cross-correlation signal which is necessary for obtaining stringent bounds on the neutrino mass. Further, one has to worry about several other observational issues like the effect of Galactic super wind. contamination from other metal lines etc. We conclude by noting that with future radio-observations of the cosmological redshifted 21-cm signal and Lyman-α forest surveys, it is possible to measure neutrino mass at a high level of precision using the cross-correlation power spectrum. We predict that the bounds obtained from such a measurement shall be competitive with other probes.